Pressure-induced amorphization of the $Y_3Ga_5O_{12}$ garnet studied to 1□Mbar

V. Monteseguro, J. Ruiz-Fuertes, M. Berkowski, G. Garbarino

PII: S0925-8388(20)31041-0

DOI: https://doi.org/10.1016/j.jallcom.2020.154678

Reference: JALCOM 154678

To appear in: *Journal of Alloys and Compounds*

Received Date: 25 October 2019

Revised Date: 4 March 2020

Accepted Date: 5 March 2020

Please cite this article as: V. Monteseguro, J. Ruiz-Fuertes, M. Berkowski, G. Garbarino, Pressure-induced amorphization of the $Y_3Ga_5O_{12}$ garnet studied to 1□Mbar, *Journal of Alloys and Compounds* (2020), doi: https://doi.org/10.1016/j.jallcom.2020.154678.

Pressure-induced amorphization of the $Y_3Ga_5O_{12}$ garnet studied to 1 Mbar

V. Monteseguro[1,2*], J. Ruiz-Fuertes[3], M. Berkowski[4], and G. Garbarino[2]

[1]*Departamento de Física Aplicada, ICMUV, Universitat de València, Dr. Moliner 50, 46100 Burjassot, Spain*

[2]*European Synchrotron Radiation Facility, BP 220, 6 Rue Jules Horowitz, 38043 Grenoble Cedex 9, France*

[3]*DCITIMAC, Universidad de Cantabria, Avenida de Los Castros 48, 39005 Santander, Spain*

[4]*Institute of Physics, Polish Academy of Sciences, Aleja Lotnikow 32/46 PL–02668 Warsaw, Poland*

Abstract

We use micro-beam synchrotron x-ray diffraction to study the pressure-induced amorphization of nano-sized and single crystals of $Y_3Ga_5O_{12}$ up to pressures exceeding 1 Mbar in static compression. The abrupt pressure-induced amorphization found for both 56 nm and bulk micrometric crystals at around 76 GPa independently of the pressure transmitting medium employed demonstrates its intrinsic nature, previously predicted at 79 GPa by *ab initio* calculations. The single crystal structural solution at 50 GPa shows that the contraction of the unit-cell, mostly accommodated by the compressible YO_8 dodecahedra, gives rise to a regularization and tilting increase of the GaO_6 polyhedra with the Y-O-Ga angle changing from 104.84º to 102.34º in 50 GPa. We obtain a bulk modulus of 178(3) GPa for the single crystal and 170(3) GPa for the nanocrystals in excellent agreement with previous calculations.

Keywords: garnets, pressure, x-ray diffraction, amorphization

*E-mail: Virginia.Monteseguro@uv.es

1. Introduction

Garnets are the most abundant group of silicate minerals constituting approximately 95% of the Earth's crust and making up the largest and most important reservoir for rock-forming minerals **[1]**. They are hard and have high optical transparency and mechanical stability. Also, their diverse chemical compositions with almost any element within the stoichiometry $A_3B_2C_3O_{12}$, and their chemical stability make these compounds perfect matrix hosts. For these reasons, garnets have been used in numerous optical applications when doped with luminescent rare earth ions. A good example is the well-known synthetic $Y_3Al_5O_{12}$ (YAG) garnet used in bulk as a laser material when doped with neodymium (Nd^{3+}). Moreover, with the current urgency on reducing the size of devices, large efforts are being put into the study of the luminescence properties of RE^{3+}-doped nanoparticles. In this scenario nanogarnets are being used for the development of new lasers for sensing and imaging in biomedicine, as an alternative to quantum dots in photonics or in optoelectronic devices for engineering **[2,3,4]**. The recent discovery by Irifune et al. **[5]** of nanocrystallization of garnets from bulk glass at high pressure and temperature conditions has boosted this research area.

Garnets crystallize in a cubic structure **[6]** with space group $Ia\bar{3}d$ and 8 formulas per unit cell, formed by a network of corner-sharing AO_8 dodecahedra, CO_4 tetrahedra, and BO_6 octahedra. In the case of $Y_3Ga_5O_{12}$ each O atom is shared with one GaO_4 tetrahedron, one GaO_6 octahedron, and two YO_8 dodecahedra. The polyhedra are arranged in chains along the three crystallographic directions forming dodecahedral cavities occupied by *A* atoms and conferring most garnets an impressively varying

Hugoniot Elastic Limit (HEL) depending on the final shock pressure **[7]**. Dynamical **[7,8,9]** and high-temperature static **[10,11]** compressions result into garnet to perovskite phase transitions at pressures above 50 GPa depending on the garnet composition. However, ambient temperature static compression gives rise to a mechanical instability predicted by calculations **[12, 13]** and a consequent pressure-induced amorphization (PIA) **[14]** except for $Ca_3Fe_2Si_3O_{12}$ where a Fe^{3+} spin-driven isosymmetric phase transition at ~60 GPa takes over **[15]**. These results indicate that the irreversible PIA process in garnets might result in the kinetic frustration of the garnet to perovskite phase transition. Usually, in order to study the PIA in garnets, the techniques chosen have been powder x-ray diffraction and Raman spectroscopy with micro-size powders **[10,16,17]**. In particular powder x-ray diffraction is strongly affected by intergrain strains, even in hydrostatic media, at high pressures. A possibility to palliate the loss of long-rage order caused by the strain is *in situ* thermally annealing with a laser. However, doing so one risks providing enough thermal energy to induce the kinetically hindered garnet to the perovskite phase transition preventing the PIA **[10]**. The information available about the mechanism of the PIA in garnets relies in powder x-ray diffraction without annealing in which accurate determination of the atomic coordinates and their thermal atomic displacements is difficult at very high pressures if not impossible. This problem could be overcome by a study with single crystal x-ray diffraction in which the available information can be extended from 1D to 3D and the strain effects are more reduced.

The objective of this study if twofold. First, we want to determine the onset pressure of the PIA of a garnet. We shall do it with $Y_3Ga_5O_{12}$ (YGG). In order to do so

we will present two experiments investigating the extremes: one experiment up to 1 Mbar with one single crystal in non hydrostatic conditions, and one experiment up to 76 GPa with nanoparticles using very high hydrostatic conditions. Nano-crystalline materials often show completely different behavior from their bulk counterparts **[18,19]**. This difference, exhaustively studied in most relevant materials as TiO_2, Y_2O_3, or PbTe, remains unexplored in garnets. Second, we shall perform a simultaneous study with both a nanopowder and a single crystal of YGG in order to follow the structure of YGG before the PIA process.

2. Experimental details

Three high-pressure angular dispersive x-ray diffraction (ADXRD) experiments were carried out at the beamline ID27 at the European Synchrotron Radiation Facility (ESRF) **[20]**. The monochromatic radiation with a wavelength of λ = 0.3738 Å was selected and the beam was focused down to 3 x 3 μm^2. Diffracted intensities were recorded with either a MAR CCD or a Perkin Elmer flat panel detector. The high-pressure experiments were performed at ambient temperature with membrane driven diamond anvil cells (mDACs) with a large opening of $4\theta \sim 64^o$. Three different pressure transmitting media, Helium (He), Neon (Ne) and KCl, were used to evaluate the effect of the pressure transmitting medium (PTM) on the experimental results. A summary of the sample types, pressure medium, and pressure calibrant of each run can be found in **Table 1**.

run	Sample type	medium	calibrant	Pressure range (GPa)

1	Single crystal	KCl	KCl	0–100
2	Nanopowder	He	Au	0–76
3	Nanopowder and single crystal	Ne	Ruby	0–50

Table 1. Experimental conditions of the x-ray diffraction experiments.

Run1 was performed at a sample to detector distance of 213.268 mm. The DAC was equipped with 100 µm diamonds and a gasket of Re pre-indented and drilled to 15 µm and 38 µm, respectively. The DAC was loaded with a ~30 µm single crystal of YGG together with KCl, which acted both as a PTM and as pressure calibrant **[21]**. Although this experiment was performed with static exposure of the sample to the X-ray beam.

Run2 was performed at a sample to detector distance of 318.17 mm. The DAC was equipped with 100 µm diamonds where a rhenium gasket pre-indented to 18 µm and drilled to 60 µm was inserted. A pellet of nanopowder YGG was loaded together with a gold chip as a pressure marker **[22,23]** and helium as PTM.

Run3 was performed at a 433.2 mm sample to detector distance. The DAC employed was equipped with 300 µm culet diamonds was used with a stainless-steel gasket, which was pre-indented to 50 µm and drilled to 160 µm. In this occasion, Ne gas was used as PTM. This cell was loaded with two samples: a 10 µm thick and 20 μm^2 single crystal and a 30 μm^2 pellet of nano-YGG. In this way, a more accurate comparison of their structural parameters can be obtained. While the powder diffraction patterns from the nano-YGG sample were obtained with static exposure of the sample to the X-ray beam, in the case of the single-crystal experiment the DAC was rocked every 1 degree in ω obtaining 64 frames. The powder frames were integrated using FIT2D **[24]** whereas the single-crystal frames were processed with the CRYSALIS^{Pro} **[25]** software for indexing reflections and intensity data reduction. The structures were

refined with SHELXL **[26]**. The pressure was determined through the ruby fluorescence method **[27].**

The two-dimensional (2D) images of run2 and run3 were also obtained by the integration of the images using the program FIT2D **[24]** to provide an intensity vs. 2θ plot. The lattice and structural parameters fittings were performed by the LeBail and Rietveld **[28,29]** refinement with the program FULLPROF **[30]**. In all the refinements, the background was defined by a linear interpolation and the profile shape was fitted by a Thompson-Cox-Hastings pseudo-Voight. The background, the full with at half-maximum (FWHM) parameters, and lattice parameters were refined.

3. Synthesis of $Y_3Ga_5O_{12}$

a. Nanopowders

Nanometer grain size powder $Y_3Ga_5O_{12}$ was synthesized by the citrate sol-gel method in air atmosphere **[15]**. Stoichiometric molar ratio of high-purity $Ga(NO_3)_3.9H_2O$ and $Y(NO_3)_3.4H_2O$ materials were dissolved in 25 ml of 1 M HNO_3 under stirring at 353 K for 3 h. Then citric acid, with a molar ratio of metal ions to citric acid of 1:2, was added to the solution, which was stirred for 2 h more and finally dried at 403 K for 36 h. This process created a gel that was fired at 673 K for 4 h in order to remove the residual nitrates and organic compounds and the subsequently obtained powder sample was finally calcined at 1073 K for 16 h. The synthesized YGG-nano has a particle-size of 56 nm obtained by the Rietveld refinement of their powder x-ray diffraction pattern measured at ambient conditions. This value agrees well with that obtained by the analysis of the HRTEM micrographs reported by Venkatramu et al. **[3]**.

b. Single crystal

Single-crystals of $Y_3Ga_5O_{12}$ (YGG-crystals) were grown by the Czochralski method using a Malvern MSR4 puller with automatic diameter control based on weighing the crucible. Starting materials - Y_2O_3 (4N) and Ga_2O_3 (5N) - were dried in 1000 °C for 4 hours before weighting. Powders in appropriate molar ratios were mixed together and then pressed into cylindrical pellets under pressure of 200 kPa and calcinated in 1350 °C for 6 hours before melting in crucible. Gallium oxide at crystal growth temperature is more volatile than yttrium oxide, and therefore its excess compared to the congruently melting composition is necessary. Applied excess of Ga_2O_3 was 0.5 mol %. Admixture of 0.3 mol % Cr_2O_3 was introduced in place of Ga_2O_3. Single crystals were grown at ambient (N_2) atmosphere on <111> oriented seed with a pulling rate of 2.5 mm/h and a speed of rotation 30 r.p.m. Transparent crystals with 20 mm diameter and 60 mm thickness were grown with a convex crystal melt interface from inductively heated iridium crucible of 40 mm in diameter. A summary of the refined structures is shown in **Table 2**.

	Experiments (this work)		**Exp.[26]**	**Calc.[15]**
P	1 atm	50.2 GPa	1 atm	1 atm
Sample form	Nano	SC	SC	
a (Å)	12.299(2)	11.5296(7)	12.273(1)	12.278
O *x*	0.098(9)	0.1012(2)	0.1007(5)	0.1
O *y*	0.193(5)	0.1891(3)	0.1954(5)	0.194
O *z*	0.279(6)	0.2794(2)	0.2774(6)	0.277
U_{iso}		0.0207(13)		
Measured refl.		1462		
Unique refl.		200		
Refined param.		9		
R_{int}		0.0965		
R1		0.0872		
wR2		0.2284		

GoodF	1.164

Table 2. Lattice parameters, oxygen atomic coordinates, and single crystal (SC) refinement and data details of our synthesized $Y_3Ga_5O_{12}$ nanogarnet at 1 atm, and our single crystal at 50.2 GPa. The structural parameters are compared with the structure at ambient conditions **[31]** and that obtained by previous *ab initio* calculations **[12]**.

4. Results and discussion

a. Amorphization of a single crystal

The amorphization of a single-crystal of YGG is studied to 1 Mbar with a routine x-ray powder diffraction experiment obtaining a limited but crucial low angle reflections (run1). The pressure evolution to 1 Mbar of this single crystal can be seen in **Fig. 1** together with diffraction rings of KCl.

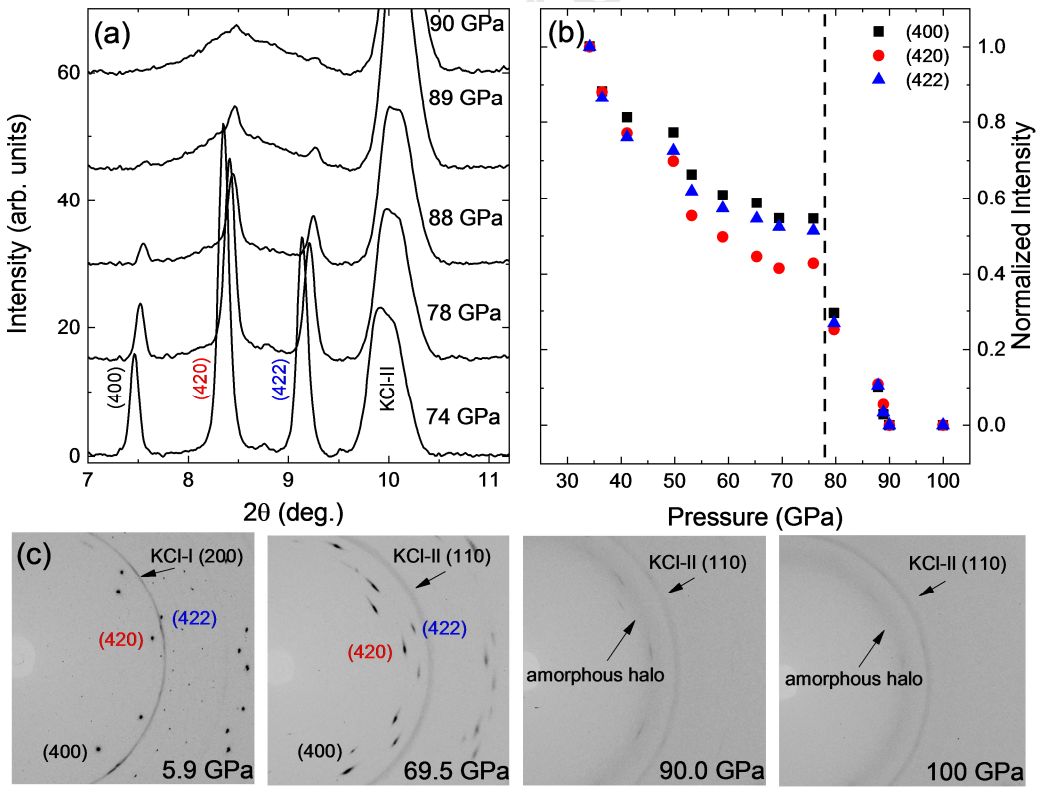

Figure 1. (run1) (a) X-ray Diffraction patterns of a single crystal of YGG (run1) above 70 GPa showing the amorphization of the crystal. The presented 2θ range also includes the (110) reflection of the KCl-II

phase. (b) Diffraction frames of the same experiment showing the evolution of the reflections while entering in the amorphous phase. The relevant (400), (420), and (422) reflections are indicated with their hkl indexes and different colors. Pressures are indicated. (c) Pressure dependence of the normalized intensity of the YGG (400), (420), and (422) reflections. Their intensities have been weighted by the intensity of the KCl-II (110) reflection, unaffected by the amorphization process of the sample.

Since the information seeked with this experiment is finding the amorphization onset of YGG with a single crystal, only a few reflections where collected at each pressure. In **Fig. 1 (a)** we show the integrated (400), (420), and (422) most intense reflections of the single crystal of YGG which include the intensities of all the measured symmetry equivalent reflections contributing to the same 2θ value. This occurs because the frame was integrated as a powder diffraction pattern to determine changes in the intensities. At 78 GPa the intensities of the three reflections drop and a broad halo located at 8.25º appears, indicating the onset of an amorphization process which ends at 90 GPa. At this pressure the three intense (400), (420), and (422) reflections disappear under this halo. The evolution of their normalized intensities is shown in **Fig. 1 (b)**. Interestingly, the intensities of the three reflections show a similar behavior under compression with a clear change above 78 GPa. Although the three reflections are not completely independent to each other, they provide information of the three crystallographic directions indicating that the amorphization mechanism takes place isotropically.

In **Fig. 1 (c)** we show a section of the diffraction frame at 5.9, 69.5, 90, and 100 GPa to indicate how the individual reflections evolve under compression. At 5.9 GPa the reflections appear rounded and well defined. At 69.5 GPa the reflections are already elongated along the 2θ ring but can still be individually located. At 90 and 100 GPa only the amorphous halo can be identified together with the ring that corresponds to the

KCl-II (110) reflection. The observed pressure-induced amorphization of YGG agrees with previous *ab initio* calculations that find a mechanical instability above 79 GPa **[12]** as the result of the violation of the Born stability criteria by the C_{44} elastic constant. The softening of the elastic shear modulus C_{44} in cubic crystals usually translates into the softening of the corresponding vibrational mode. In **Ref. [12]** it is shown that for YGG the mode that softens is a T_{2u} silent mode but its frequency becomes imaginary above the mechanical instability.

b. Amorphization of a nanopowder

A selection of the x-ray powder diffraction patterns of 56-nm sized nanoparticles of YYG is shown in **Fig. 2** (run2).

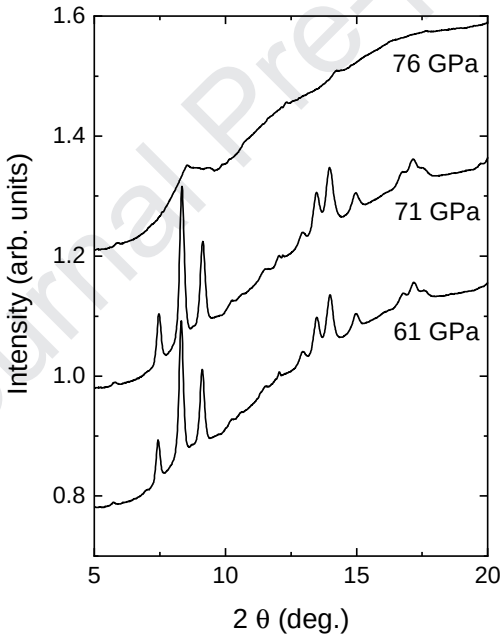

Fig. 2. (run2) X-ray diffraction patterns of nanopowder of YGG (~56 nm in size) above 60 GPa showing the amorphization of the sample at 76 GPa. In this case, He was employed as pressure transmitting medium and pressure was determined by Au.

According to previous *ab initio* calculations **[6]**, the YGG garnet is very stable and it starts to suffer mechanical instability at 79 GPa. Under compression, the intensities of the reflections start to decrease while their width continuously increase. At 71 GPa, the spatial coherence of the nanoparticles still remains. At 76 GPa the disappearance of reflections and the appearance of a halo indicate the complete and abrupt amorphization of the sample, in excellent agreement with our previous single-crystal x-ray diffraction experiment performed in KCl and previous *ab initio* calculations **[6]**. The use of different pressure transmitting media does not allow direct comparison between the single-crystal experiment shown above (run1) and the experiment with nanopowders in He (run2). However, the almost identical amorphization onset obtained by both experiments and its agreement with previous calculations indicate that the PIA process in YGG is independent of the sample size and pressure medium used.

c. Behavior of the crystalline phase

In order to obtain information about the behavior of a single crystal and a nanopowder of YGG about its compressibility and behavior just before the PIA we have performed a simultaneous study with both sample types up to 50 GPa using Ne as pressure transmitting medium (run3). The diffraction pattern of nano-YGG and the reconstructed reciprocal space of a single crystal of YGG projected along the b^*c^* plane at 50 GPa are shown in **Fig. 3.**

The PIA process in garnets is intrinsic as has been confirmed in run1 and run2 where the amorphization onset pressure is shown to be independent of the grain size or the pressure medium. However, in **Fig. 3 (a)** one can see that under compression both

the intensity decreases and the width of the reflections increases dramatically even several GPa before the PIA. We shall analyze the causes now.

When the crystal size and its surface are comparable as in nanocrystals (ours are ~56 nm in size), the surface defects play an important role. Previous works **[32]** have demonstrated that under compression, even in hydrostatic conditions, the number of defects in the surface tends to increase, which in addition to the appearance of inhomonegeous strain even at hydrostatic conditions translates into a rapid deterioration of the XRD diffraction pattern as observed in **Fig. 3**.

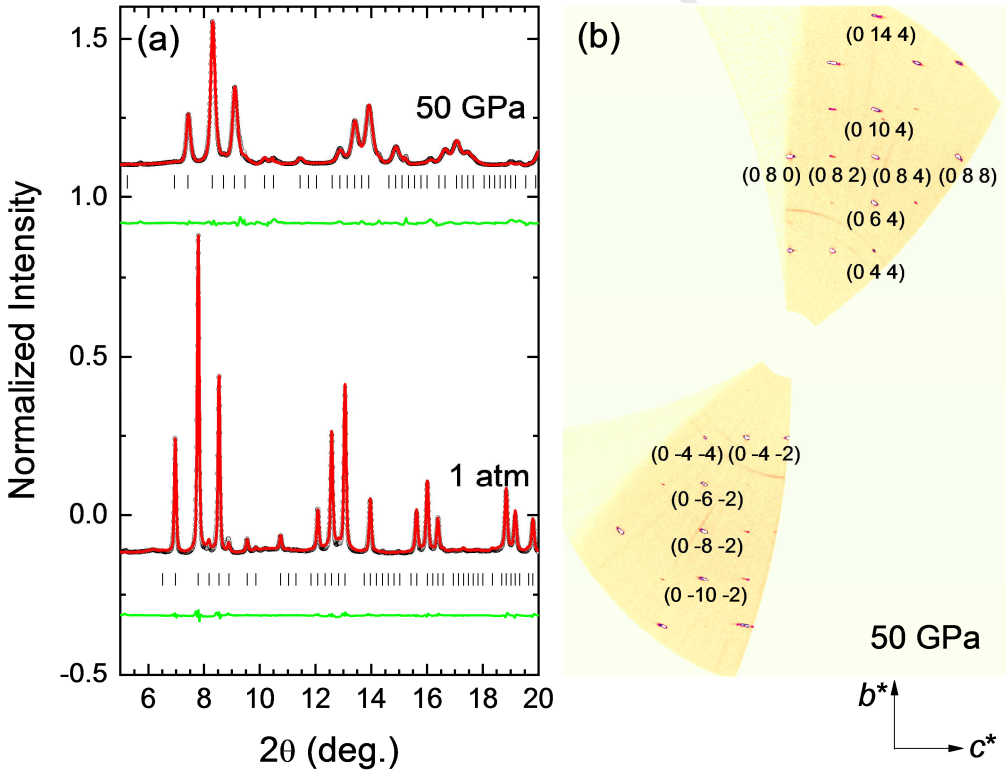

Fig. 3. (run3) (a) Powder XRD patterns of nano YGG at ambient pressure, and 50 GPa. The dots are experimental points and the continuous lines are the Rietveld fits (red) and the experimental to fit difference (green). (b) Reconstruction of the reciprocal space along the *b***c** directions. The reflections, although elongated are still good and allowed an anysotropycal refinement of the structure.

According to Hall **[33]**, the dependence of both broadening contributions with the diffracting angle θ can be separated since the size-associated broadening varies as 1/cosθ and the strain-associated broadening does as tanθ, according to $\beta_t = C\,\varepsilon\,\tan\theta + K\lambda/L$. Here, C and K are constants, ε is the strain, λ is the x-ray wavelenght and *L* is the crystalline grain size. In **Fig. 4 (a)** we show the Williamson-Hall plot **[33]** at ambient pressure and 35 GPa from run 3 to illustrate the evolution of the grain size and broadening strain suffered by our YGG nanoparticles.

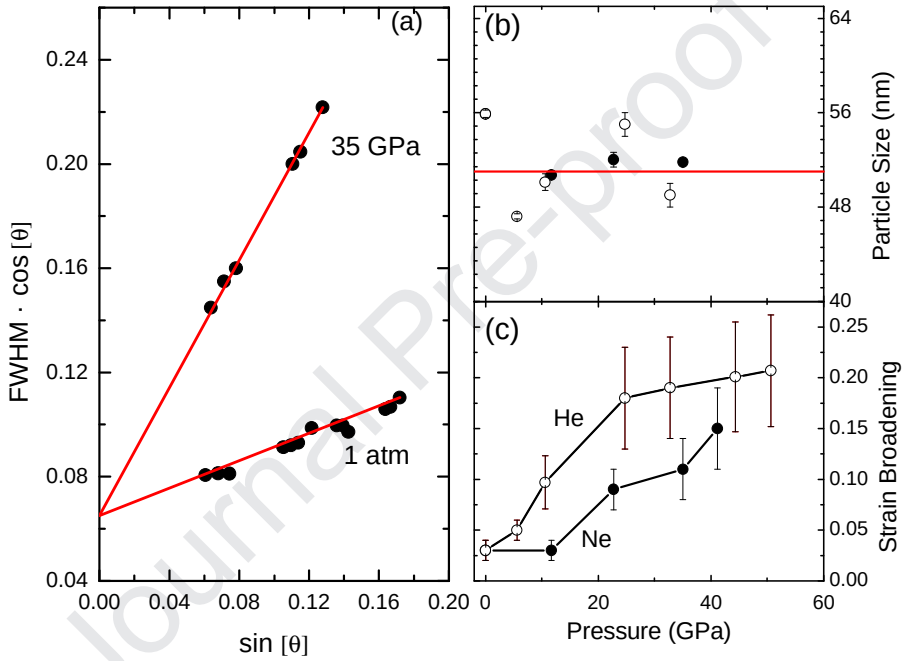

Fig. 4. (a) Williamson-Hall plot at 1 atm and 35 GPa in the experiment with Ne as pressure transmitting medium. The red continuous lines are linear fits. (b) Pressure-dependence of the particle size and (c) of the Strain Broadening in both run 2 and run 3 using Ne and He as pressure transmitting medium, respectively.

One can see that under compression the dependece of the [FWHM × cos θ] product for isolated reflections at different 2θ positions changes its dependence with the sin θ. Such a slope change indicates a considerable pressure-increase of the broadening strain as shown in **Fig. 4 (c)** independently of the pressure transmitting medium. However,

the intercept of the straight line is found to be pressure independent indicating that the particle size, and therefore the crystalline to amophous ratio remains constant under compression, within the uncertainties [**Fig. 4 (b)**] at least up to the onset of the PIA.

As explained above, the PIA process in YGG is due to the mechanical instability caused by the softening of the C_{44} element of the strain tensor. Such a softening is complex to see even after performing an anisotropic refinement of single crystal x-ray diffraction data. According to Gavriliuk et al. **[34]** the location of the amorphous halo of $Y_3Fe_5O_{12}$ indicates that its short-range order consists of FeO_6 octahedral blocks with disordered orientations. This idea is also used to explain the PIA process in $Eu_3Ga_5O_{12}$. In this case the combination of x-ray diffraction, Raman spectroscopy and Eu^{3+} luminescence serve to conclude that the PIA process is due to the overlapping of the Ga tetrahedra and octahedra **[16]**. That overlapping gives rise to an increase of the asymmetry of the oxygen local environment of Eu^{3+}. In our study with a single crystal we have performed two experiments. The first one (run1) we have gone to 1 Mbar but in this experiment the number of measured reflections ~10 was not enough to refine the structure. In the second experiment with a single crystal (run3) [**Fig. 3(b)**] we collected 1462 reflections but the experiment had to be terminated at 50 GPa, rather before the PIA which was found to be at 76 GPa. The softening of the C44 element has a vibrational mode associated to it. In particular, it is the triple degenerated T_{2u} silent mode which becomes imaginary above 111 GPa **[35].** The frequency of this mode at ambient pressure is of 109 cm^{-1} and according to Chaplin et al. **[36]** it is a translational mode of Y^{3+} with the oxygen framework at rest. The single-crystal diffraction data obtained at 50 GPa allowed us to carry out an anisotropic structural refinement

performed with the 1462 collected reflections, 200 of them unique, with an internal R_{int} value of ~10% as shown in **Table 2**. Since the silent T_{2u} mode starts to rapidly soften above 20 GPa, we should already notice such motion in the thermal displacement parameters of the oxygen atoms at 50 GPa. The equivalent atomic displacement parameters U_{eq} found at 50 GPa are 0.0153(8) Å^2, 0.0156(9) Å^2, 0.0152(9) Å^2, and 0.21(2) Å^2 for Y, Ga1, Ga2, and O, respectively. These results indicate, as expected, that one the one hand the oxygen atoms have higher thermal displacement parameters than the Y and the two Ga ions, and on the other hand it also indicates that at this pressure all the atoms of YGG remain rather still at their sites. However, when we look at the off-diagonal elements of the thermal displacement tensor of the four atomic sites we find that they are zero except the Y U_{23} = 0.0011(2) Å^2 and the O U_{13} = 0.002(1) Å^2. Therefore, both sites present anisotropic motion. Even though 50 GPa is still a pressure too low to evaluate the effects of PIA this result supports the conclusions of Lin et al. **[16].** The PIA process in garnets originates as an asymmetry increase of the oxygen local environment of Y^{3+}. The dramatic shortening of the distances between polyhedra further supports this. According to our structural solution at 50 GPa with single-crystal x-ray diffraction, the distance between the YO_8 dodecahedra and the GaO_4 tetrahedra changes from 3.4304(2) Å at ambient pressure to 2.8824(2) Å at 50 GPa. At a Eu–Ga distance of ~2.85 Å (~85 GPa) $Eu_3Ga_5O_{12}$ amorphizes **[16]**.

In garnets the compression mechanism can be dominated either by bond compression or polyhedral rotation **[37]**. The structural refinement of the structure at 50 GPa yields atomic coordinates for oxygens which vary a maximum of 3% from those at ambient pressure. This indicates the robustness of the crystal structure. The Y-O

distances in the irregular YO_8 dodecahedra are 2.35 and 2.42 Å at ambient pressure, while the Ga-O distances are 2.03 Å and 1.83 Å in GaO_6 and GaO_4, respectively. However, at 50 GPa, as obtained from the structural solution of the high-pressure single crystal data shown in **Table 2**, the Y-O distances are 2.22 and 2.24 Å, while the Ga-O distances reduce to 1.89 and 1.75 Å in GaO_6 and GaO_4, respectively. Regarding the distortion Y-O-Ga angle it changes from 104.84º at ambient pressure to 102.34º at 50 GPa. Therefore, in YGG compression involves both a regularization of the YO_8 dodecahedra and a tilting increase of the GaO_6 octahedra. This must be the mechanism to reduce the Y-Ga distance so much under compression.

In **Fig. 5** we show the pressure dependence of the YGG polyhedral volumes obtained in run 3 since those are the only diffraction patterns that allowed us to perform reliable Rietveld refinements at least up to 30 GPa, which is the hydrostatic limit in Ne **[38]**.

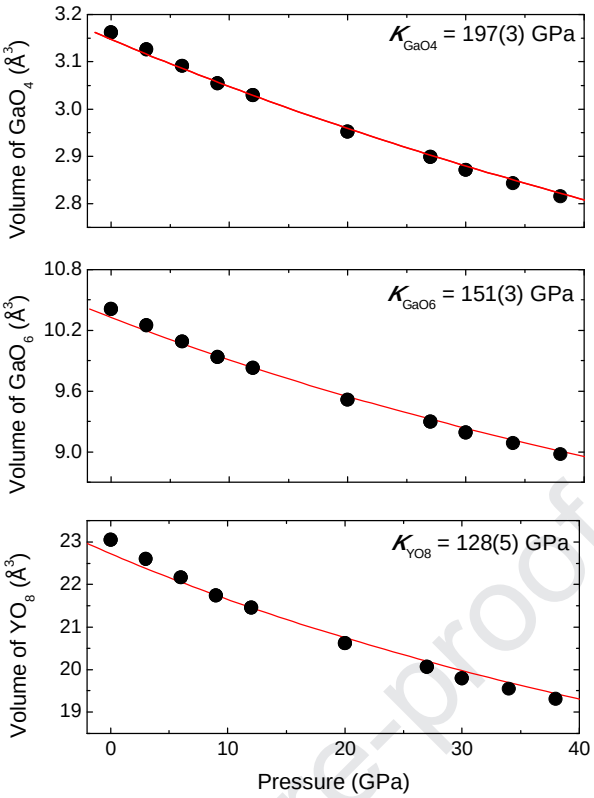

Fig. 5. Pressure dependence of the polyhedral volume of $Y_3Ga_5O_{12}$. The points are the data obtained in the hydrostatic limit in run 3. The red continuous lines are the fits to second-order Birch-Murnahan equations of state **[38]**. The individual bulk moduli are also shown.

The pressure-volume curves of the polyhedra were fitted according to a second order Birch-Murnaghan **[39]** EoS since fits to third order EoS provided unrealistic pressure derivatives of the bulk modulus. The bulk moduli (**Table 2**) indicate that most of the compression is accommodated by the YO_8 dodecahedra, being the GaO_4 tetrahedra the most incompressible units. According to Milman et al. **[37]** the bulk modulus in garnets can be correlated to the bulk modulus of their dodecahedra according to K_0 = 35 GPa + 1.05·$K_0(YO_8)$, which in the case of YGG would lead to a bulk modulus of 169 GPa.

The pressure dependence of the unit-cell volume of YGG is shown in **Fig. 6** for the data obtained for both nano and single crystal YGG. The theoretical pressure-volume dependence is also shown for comparison.

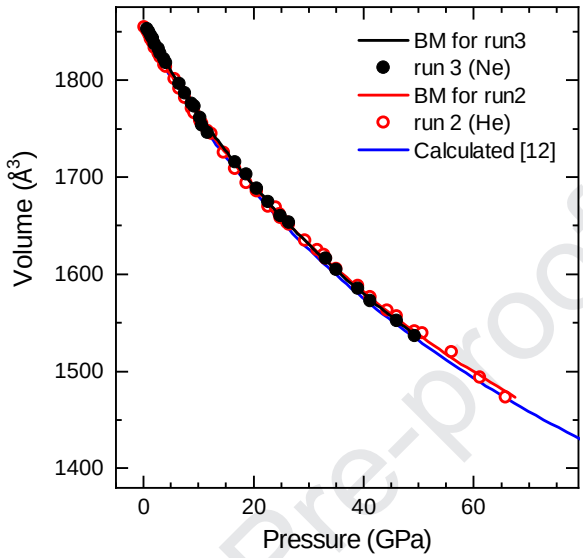

Fig. 6. Pressure dependence of the unit-cell volume of the $Y_3Ga_5O_{12}$. Blacks dots correspond to volume values obtained from the nanopowder in run3 and red dots are volume points obtained from run2. The red and black solid lines correspond to second order Birch-Murnaghan EoS fits **[38]**. The blue line correspond to the calculated EoS in **Ref. [12]**.

The obtained results after performing independent second order BM EoS fits are shown in **Table 2**. The agreement with the proposed correlation between K_0 and K_{YO8} by Milman et al. **[37]** is excellent demonstrating that independently of the chemical formula garnets relay most of their compression on that of their dodecahedra.

	V_0 (Å^3)	K_0 (GPa)	K_{YO8} (GPa)	K_{GaO6} (GPa)	K_{GaO4} (GPa)
Single crystal	1859.1(8)	178(3)			
Nano	1859(1)	172(3)	128(5)	151(3)	197(3)
Calc. **[12]**	1853	170			

Table 2. Ambient pressure volume and bulk moduli of $Y_3Ga_5O_{12}$ and its polyhedral obtained by x-ray diffraction from single-crystal and nano forms and compared with previous calculations.

5. Conclusions

The pressure-induced amorphization (PIA) of $Y_3Ga_5O_{12}$ (YGG) nano-garnet (56 nm) has been compared with its homologous single-crystal (20 µm) YGG up to 100 GPa. It has been found that the PIA of YGG is both grain-size and pressure medium independent occurring at ~76 GPa. That result agrees very well with the previously calculated value **[12]** which predict a mechanical instability at 79 GPa. The amorphization pressure of the YGG compares very well with the amorphization onset of other garnets as GGG (84(4) GPa) and GSGG (58(3) GPa) **[14]**. The anisotropic structural refinement of our single crystal x-ray diffraction experiment at 50 GPa has confirmed previous conclusions **[16]** that establish that the mechanism of the PIA process in garnets is the result of a strong reduction of the inter YO_8 and GaO_4 polyhedral distances. Such a reduction produces and overlapping of both coordination blocks that results in a PIA. The volume-pressure curves of YGG have been fitted by a second-order BM EoS. The obtained values for the room pressure volume and the bulk modulus are in very good agreement with previous calculations.

Acknowledgements

V. M. and J.R-F. thank the Ministry of Science, Innovation and Universities for the Juan de la Cierva program (FJCI-2016-27921) and for project PGC-2018-097520-A-100, respectively. The authors would like to acknowledge M. Mezouar for the inhouse

beamtime allocation and fruitful discussions, to J. Jacobs (High Pressure Lab.) for the preparation of the DACs.

References

[1] Mahmoud, A.; Erba, A.; Doll, K.; Dovesi, R. Pressure effect on elastic anisotropy of crystals from ab initio simulations: the case of silicate garnets. *J. Chem. Phys.* **2014**, *140*, 234703.

[2] Jaque, D.; Vetrone, F. Luminescence Nanothermometry. *Nanoscale* **2012**, *4*, 4301.

[3] Venkatramu, V.; León-Luis, S. F.; Rodríguez-Mendoza, U. R.; Monteseguro, V.; Manjón, F. J.; Lozano-Gorrín, A. D.; Valiente, R.; Navarro-Urrios, D.; Jayasankar, C. K.; Muñoz, A.; Lavín, V**.** Synthesis, Structure and Luminescence of Er^{3+}-Doped $Y_3Ga_5O_{12}$ Nano-Garnets*. J. Mater. Chem.* **2012**, *22*, 13788.

[4] León-Luis, S. F.; Monteseguro, V.; Rodríguez-Mendoza, U. R.; Rathaiah, M.; Venkatramu, V.; Lozano-Gorrín, A. D.; Valiente, R.; Muñoz A.; Lavín, V. Optical nanothermometer based on the calibration of the Stokes and upconverted green emissions of Er^{3+} ions in $Y_3Ga_5O_{12}$ nano-garnets. *RSC Adv.* **2014**, *4*, 57691.

[5] Irifune, T.; Kawakami, K.; Arimoto, T.; Ohfuji, H.; Kunimoto, T.; Shinmei, T. Pressure-induced nano-crystallization of silicate garnets from glass. *Nat. Commun.* **2016**, *7*, 13753.

[6] Menzer, G. Z. The crystal structure of garnet. *Kristallogr.* **1926**, *63*, 157.

[7] Zhou, X.; Li, J.; Nellis, W. J.; Wang, X.; Li, J.; He, H. Pressure-dependent Hugoniot elastic limit of $Gd_3Ga_5O_{12}$ single crystals. *J. Appl. Phys.* **2011**, *109*, 083536.

[8] Kishimura, H.; Matsumoto, H. Structural evolution of $Y_3Fe_5O_{12}$ induced by shock compression. *Jap. J. Appl. Phys*. **2017**, *56*, 105601.

[9] Mashimo, T.; Chau, R.; Zhang, Y.; Kobayoshi, T.; Sekine, T.; Fukuoka, K.; Syono, Y.; Kodama, M.; Nellis, W. J. Transition to a Virtually Incompressible Oxide Phase at a Shock Pressure of 120 GPa (1.2 Mbar): $Gd_3Ga_5O_{12}$. *Phys. Rev. Lett.* **2006**, *96*, 105504.

[10] Lin, C.; Liu, J.; Lin, J. F.; Li, X.; Li, Y.; Zhang, Q.; Xiong, L.; Li, R. Garnet-to-Perovskite Transition in $Gd_3Sc_2Ga_3O_{12}$ at High Pressure and High Temperature. *Inorg. Chem.* **2013**, *52*, 431.

[11] Stan, C. V.; Wang, J.; Zouboulis, I. S.; Prakapenka, V.; Duffy, T. S. High-pressure phase transition in $Y_3Fe_5O_{12}$. *J. Phys.: Condens. Matter.* **2015**, *27*, 405401.

[12] Monteseguro, V.; Rodríguez-Hernández, P.; Lavin, V.; Manjón, F.J.; Muñoz, A. Electronic and Elastic Properties of Yttrium Gallium Garnet under Pressure from Ab Initio Studies. *J. Appl. Phys.* **2013**, *113*, 183505.

[13] Monteseguro, V.; Rodríguez-Hernández, P.; Ortiz, H. M.; Venkatramu, V.; Manjón, F. J.; Errandonea, D.; Jayasankar, C. K.; Muñoz, A. Structural, elastic and vibrational properties of nanocrystalline lutetium gallium garnet under high pressure. *Phys.Chem.Chem.Phys.*, **2015**, *17*, 9454.

[14] Hua, H.; Mirov, Sergey B.; Vohra, Y. K. High-Pressure and High-Temperature Studies on Oxide Garnets. *Phys. Rev. B.* **1996**, *54*, 6200.

[15] Friedrich, A.; Winkler, B.; Morgenroth, W.; Ruiz-Fuertes, J.; Koch-Müller, M.; Rhede, D.; Milman, V. Pressure-induced spin collapse of octahedrally coordinated Fe^{3+} in $Ca_3Fe_2[SiO_4]_3$ from experiment and theory. *Phys. Rev. B.* **2014**, *90*, 094105.

[16] Lin, C. L.; Li, Y. C.; Li, X. D.; Li, R. Li, Lin, J. F.; Liu, J. Pressure-induced structural evolution and amorphization in $Eu_3Ga_5O_{12}$. *J. Appl. Phys.* **2013**, *114*, 163521.

[17] Hua, H.; Liu, J.; Vohra, Y. K. Pressure-induced amorphization in gadolinium scandium gallium garnet by x-ray diffraction and spectroscopic studies. J. Phys.: Condens. Matter. **1996**, *8*, 139.

[18] Swamy, V.; Kuznetsov, A.; Dubrovinsky, L. S.; McMillan, P. F.; Prakapenka, V. B.; Shen, G.; Muddle, B. C. Size-Dependent Pressure-induced Amorphization in Nanoscale TiO_2. Phys. Rev. Lett. **2006**, *96*, 135702.

[19] Machon, D.; Melinon, P. Size-dependent pressure-induced amorphization: a thermodynamic panorama. Phys. Chem. Chem. Phys. **2015**, *17*, 903.

[20] Mezouar, M.; Crichton, W. A.; Bauchau, S.; Thurel, F.; Witsch, H.; Torrecillas, F.; Blattmann, G.; Marion, P.; Dabin, Y.; Chavanne, J.; Hignette, O.; Morawe C.; Borel, C. Development of a new state-of-the-art beamline optimized for monochromatic single-crystal and powder X-ray diffraction under extreme conditions at the ESRF. *J. Synchrotron Rad.* **2005**, *12*, 659.

[21] Dewaele, A.; Belonoshko, A. B.; Garbarino, G.; Occelli, F.; Bouvier, P.; Hanfland, M.; Mezouar, M. High-pressure-high-temperature equation of state of KCl and KBr. *Phys. Rev. B.* **2012**, *85*, 214105.

[22] Takemura K.; Dewaele, A. Isothermal equation of state for gold with a He-pressure medium. *Phys. Rev. B.* **2008**, *78*, 104119.

[23] Dorogokupets, P. I.; Oganov, A. R. Ruby, metals, and MgO as alternative pressure scales: A semiempirical description of shock-wave, ultrasonic, x-ray, and thermochemical data at high temperatures and pressures. *Phys. Rev. B.* **2007**, *75*, 024115.

[24] Fit2D, http://www.esrf.eu/computing/scientific/FIT2D/

[25] Agilent, CRYSALIS^{Pro} software system, version 1.171.39.46, Agilent Technologies UK Ltd. Oxford, UK, 2018.

[26] Sheldrick, G. M. A short history of SHELX. *Acta Crystallogr., Sect. A.* **2008**, *64*, 112.

[27] Silvera, I. F. ; Chijiote, A. D. ; Nellis, W. J.; Soldatov, A. ; Tempere, J. Calibration of the ruby pressure scale to 150 GPa. *Phys. Stat. Sol(b)* **2007**, *244*, 460.

[28] LeBail, A. Whole Powder Pattern Decomposition Methods and Applications: A Retrospection. *Powder Diffraction*. **2005**, *20*, 316.

[29] Rietveld. H. M. A profile refinement method for nuclear and magnetic structures. *J. Appl. Cryst.* **1969**, *2*, 65.

[30] Rodríguez-Carvajal, J. Recent developments of the program FULLPROF, *Commission on powder diffraction (IUCr). Newsletter*. **2001**, *26*, 12.

[31] Nakatsuka, A.; Yoshiasa A.; Takeno, S. Site preference of cations and structural variation in $Y_3Fe_{5-x}Ga_xO_{12}$ ($0 \leq x \leq 5$) solid solutions with garnet structure. *Acta Cryst. Section B.* **1995,** *51*, 737.

[32] Ruiz-Fuertes, J.; Gomis, O.; León Luis, S.F.; Schrodt, N.; Manjón, F. J.; Ray, S.; Santamaría-Pérez, D.; Sans, J.A. Ortiz, H. M.; Errandonea, D.; Ferrer-Roca, C.; Segura, A. Martínez-García, D.; Lavin, V.; Rodríguez-Mendoza, U. R.; Muñoz, A. Pressure-induced amorphization of YVO_4:Eu^{3+} nanoboxes. *Nanotechnology* **2016**, *27*, 025701.

[33] Williamson, G. K.; Hall, W. H. X-ray line broadening from filed aluminum and wolfram. *Acta Metall*. **1953**, *1*, 22.

[34] Gavriliuk, A. G.; Struzhkin, V. V.; Lyubutin, I. S.; Eremets, M. I.; Trojan, I. A.; Artemov, A. A. *JETP Lett.* **2006**, *83*, 37.

[35] Monteseguro, V.; Rodríguez-Hernández, P.; Vilaplana, R.; Manjón, F. J.; Venkatramu, V.; Errandonea, D.; Lavín, V.; Muñoz, A. Lattice Dynamics Study of Nanocrystalline Yttrium Gallium Garnet at High Pressure. *J. Phys. Chem. C*. **2014**, *118*, 13177.

[36] Chaplin, T.; Price, G. D.; Ross, N. L. Computer simulation of the infrared and Raman activity of pyrope garnet, and assignment of calculated mode to specific atomic motions. *American Mineralogist* **1998**, *83*, 841.

[37] Milman, V.; Akhmatskaya, E. V.; Nobes, R. H.; Winkler, B.; Pickard, C. J.; White, J. A. Systematic ab initio study of the compressibility of silicate garnets. Acta Cryst. B **2001**, *57*, 163.

[38] Klotz, S.; Chervin, J.C.; Munsch, P.; Le Marchand, G. Hydrostatic limits of 11 pressure transmitting media. *J. Phys. D: Appl. Phys.* **2009**, *42*, 075413.

[39] Birch, F. Finite Elastic Strain of Cubic Crystals. *Phys. Rev.* **1947**, *71*, 809

- Micro-beam synchrotron x-ray diffraction up to 1 Mbar.
- Comparative simultaneously 56 nm and bulk micrometric $Y_3Ga_5O_{12}$ garnet crystals.
- Pressure-induced amorphization does not depend neither pressure-transmitting medium or crystal size.
- Independently of the chemical formula garnets relay most of their compression on that of their dodecahedra.

V.M. and G.G. designed and performed the experiments. V.M. analyzed the powder x-ray diffraction data, J.R.-F. analyzed the single crystal x-ray diffraction data. M. B. synthesized the samples. V. M. and J.R.-F. wrote the manuscript.

Declaration of interests

☒ The authors declare that they have no known competing financial interests or personal relationships that could have appeared to influence the work reported in this paper.

☐The authors declare the following financial interests/personal relationships which may be considered as potential competing interests: